ELSEVIER

Contents lists available at ScienceDirect

Energy & Buildings

journal homepage: www.elsevier.com/locate/enb



Fifty shades of grey: Automated stochastic model identification of building heat dynamics



Julien Leprince ^{a,*}, Henrik Madsen ^b, Clayton Miller ^c, Jaume Palmer Real ^b, Rik van der Vlist ^d, Kaustav Basu ^d, Wim Zeiler ^a

- ^a Technical University of Eindhoven, 5 Groene Loper, Eindhoven 5600 MB, The Netherlands
- ^b Technical University of Denmark, Building 303B Matematiktorvet, Lyngby 2800, Denmark
- ^cNational University of Singapore, 11 Kent Ridge Drive, Singapore 119244, Singapore
- ^d Eneco, 5 Marten Meesweg, Rotterdam 3068 AV, The Netherlands

ARTICLE INFO

Article history: Received 23 December 2021 Revised 17 March 2022 Accepted 9 April 2022 Available online 20 April 2022

Keywords:
Buildings
Automation
Grey-box models
Heat dynamics
Scalable approaches
Performance benchmarks

ABSTRACT

To reach the carbon emission reduction targets set by the European Union, the building sector has embraced multiple strategies such as building retrofit, demand side management, model predictive control and building load forecasting. All of which require knowledge of the building dynamics in order to effectively perform. However, the scaling-up of building modelling approaches is still, as of today, a recurrent challenge in the field. The heterogeneous building stock makes it tedious to tailor interpretable approaches in a scalable way. This work puts forward an automated and scalable method for stochastic model identification of building heat dynamics, implemented on a set of 247 Dutch residential buildings. From established models and selection approach, automation extensions were proposed along with a novel residual auto-correlation indicator, i.e., normalized Cumulated Periodogram Boundary Excess Sum (nCPBES), to classify obtained model fits. Out of the available building stock, 93 building heat dynamics models were identified as good fits, 95 were classified as close and 59 were designed as poor. The identified model parameters were leveraged to estimate thermal characteristics of the buildings to support building energy benchmarking, in particular, building envelope insulation performance. To encourage the dissimination of the work and assure reproducibility, the entire code base can be found on Github along with an example data set of 3 anonymized buildings. The presented method takes an important step towards the automation of building modeling approaches in the sector. It allows the development of applications at large-scale, enhancing building performance benchmarks, boosting city-scale building stock scenario modeling and assisting end-use load identifications as well as building energy flexibility potential estimation.

© 2022 The Author(s). Published by Elsevier B.V. This is an open access article under the CC BY license (http://creativecommons.org/licenses/by/4.0/).

1. Introduction

In a context of global carbon emission reduction, the building sector has embraced data as the new fuel to harvest, at scale, the power of building performance modeling, granting valuable insights into the dynamics driving the energy demand of buildings. Indeed, while holding a share of up to 39% of global emissions in 2018 [1], the building sector has investigated multiple strategies over the last decade to reduce, adapt and better anticipate its energy load on the power network. Well established techniques

E-mail addresses: j.j.leprince@tue.nl (J. Leprince), hmad@dtu.dk (H. Madsen), clayton@nus.edu.sg (C. Miller), jpre@dtu.dk (J.P. Real), rik.vandervlist@eneco.com (R. van der Vlist), kaustav.basu@eneco.com (K. Basu), w.zeiler@tue.nl (W. Zeiler).

such as building retrofitting [2], demand side management [3], energy forecasting [4], and building to grid energy management schemes emerging from model predictive control [5] or reinforcement learning [6], have, and still are, at the center of a considerable amount of attention from both research and industry. All, however, require knowledge of the building thermal dynamics in order to effectively perform, consequently placing our ability to effectively identify building thermal behavior(s) as the backbone of building applications. Yet, despite its momentum, building modelling is still faced with the fundamental challenge of scaling across the heterogeneous building stock, and relies primarily on assumptions rather than field performance data.

Main existing modeling methods can be divided in three preeminent categories: physics-based methods (white-box), purely data driven (black-box) and hybrid approaches (grey-box) [7].

^{*} Corresponding author.

The first, physics and knowledge-based models, solves mathematical equations based on physical laws to characterize the energy behavior of buildings. They require exhaustive information on the building and are usually mathematically complex. Yet, they can yield high accuracies if calibrated correctly and are often employed in building performance simulation softwares, e.g., Energy-Plus [8], or using powerful modelling languages, e.g., Modelica [9]. White-box modeling, however, is time-consuming with performances largely depending on accurate energy model calibration consequently making it difficult to scale-up. It requires the definition and update of many input parameters along the building's lifetime [10], a process reliant on expert analysis that needs repetition for every considered building. Moreover, their copious amount of parameters makes white-box models non structurally identifiable, which often becomes problematic when an unknown parameter needs estimating. The second category constitutes data driven models, often referred to as black-box models. They consist of statistical regressions and machine learning algorithms typically fitted on the input and output time-series data of the system. Its 'black-box' analogy stresses the relationship between model input and output as being hardly transposable to physics-based analysis, making it challenging to produce interpretable models [7]. While significant developments in this field might alleviate the persisting barriers of domain knowledge inclusion or interpretability, progress is still desperately needed for trust-worthy and scalable applications within the building sector. Lastly, machine learning approaches require large amounts of quality data to guarantee satisfying accuracies of models from training. This implies data consistency, assessing coherent matching of various attributes, data completeness (no missing values) and accuracy (absence of outliers) [11]. Finally, grey-box models work as a hybrid approach between the aforementioned datadriven and physics-based models. This approach profits from dominant physical properties of the system to build the model structure while employing measurements to fix the model parameters. A common approach to modeling building heat dynamics adopts lumped resistance-capacity models, i.e. RC models, resulting in an electric circuit representation of the thermal conditions of the building [12]. In this way, grey-box approaches capitalize on the inclusion of physical knowledge in their models. This results in smaller amounts of required experimental data to train the model compared to black-box, thus making grey-box models better at generalization while staying interpretable [13].

A common problem with model identification lies in finding a model in agreement with both the physical reality as well as the level of information embedded in the data, meaning the model should avoid both under-fitting and over-fitting the measurements. To tackle this, Bacher and Madsen [14] suggested an extensive stochastic model identification procedure to identify building heat dynamics from numerous RC models of different orders. Models were evaluated based on likelihood ratio tests and selection procedure was carried out through significance improvement evaluation from simpler to more complex models, to avoid over-fits in the model selection phase. It was argued by Yu et. al. [10] that firstand (simple) second-order models are sufficient to capture the thermal dynamics of buildings to fend off the aforementioned problem. The research foundation for this claim is, however, built upon findings emerging either from simulated data sets or fairly simple and isolated single building measurements. Our intuition would argue that to determine the dynamics of real-world occupied buildings from measurements, larger model orders are not only relevant but necessary to encapsulate the, often different, thermal inertiae of buildings and bring forth most-needed comprehensive thermal behavioral insights. Assuming low-order models without the consideration of higher-order ones is, within our field, a judgmental bias that desperately needs tackling. As of today, there is very little work studying building model identification from large and occupied building stocks. Hossain et. al. [15] notably evaluated the performance of Bayesian neural networks for *nRnC* grey-box thermal model identification from 8'834 Canadian homes with 3 months worth of data. Their study demonstrated the value brought by transfer learning for smaller available building data sets as well as the overall better performance of their Bayesian approach to other black-box models based on root-mean squared errormetric. Yet, R and C parameters of the fitted models could not be uniquely identified. This, prevents the physical interpretation of parameters in the model evaluation phase, a step most studies do not comment on, along with the identifiability of their assumed model structures as mentioned by Deconinck and Roels [16].

1.1. Motivation

This paper proposes to put forth an automated model selection and evaluation procedure for stochastic model identification of building heat dynamics, providing a much needed scalable method tailored to the existing heterogeneous residential building stock. Leveraging the procedure proposed by Bacher and Madsen [14], RC models of rising complexity are evaluated over 247 Dutch residential buildings. Identified thermal parameters are then examined and employed to support building envelope performance analysis; providing large scale, non-intrusive insulation insights into the existing building stock. Important application perspectives to the approach are finally provided illustrating the impact of building model identification from measurements at scale.

The rest of the article is organized as follows. Description of the applied grey-box method, along with the proposed model selection and evaluation procedure is described in Section 2. Section 3 presents the implementation specifics of the work where building stock and climate characteristics are reported. Section 4 details the results of the model selection and evaluation procedure together with estimated parameter characteristics and building envelope performance benchmarking. Lastly, application perspectives are detailed in Section 5, and Section 6 concludes the article.

2. Methodology

This section first describes the formulation of stochastic differential equations for building heat dynamics modeling. Evaluated RC models are then detailed followed by the automated model selection and evaluation procedure.

2.1. Grey-box models of a dynamic system

Using prior physical knowledge as well as information embedded in data, grey-box models are established by sets of partially observed first-order stochastic differential equations, also referred to as stochastic linear state-space models in continuous-discrete time. These equations describe lumped RC models of the heat dynamics of the building. Typically building thermal models consider the heat exchanges between inside and outside conditions, i.e., temperature differences, solar radiation gains but can also include long wave radiations, as well as convection and infiltration driven by wind-speed if available data permits it [17]. The building envelope consequently embodies the most crucial component of the model, regulating heat transfers between these two environments. Further, diverse indoor components such as space-heating inertia, measurement errors present in the input variables and additional building zones are modelled using additional temperature state points.

We refer to the work of Bacher and Madsen [14] for the developed models as well as their evaluation and selection procedure. A

typical first-order stochastic differential equation can be expressed

$$dT_{i} = \frac{1}{R_{ia}C_{i}}(T_{a} - T_{i})dt + \frac{1}{C_{i}}\Phi_{h}dt + \frac{1}{C_{i}}A_{w}\Phi_{s}dt + \sigma_{i}d\omega_{i}, \tag{1}$$

where T, R and C refer to temperature, resistance and capacitor respectively, while Φ is an energy flux and A_w the window area. The subscript i points to the inside temperature, while a refers to the ambient temperature, h to the heater and s to solar. ω describes a standard Wiener process, and σ stands for the incremental variances of the Wiener process which encapsulate model approximations and non-recognized or modeled phenomena [18].

This physical part of the model is coupled to a data-driven one, linking the data observations to the model for parameter estimation. The discrete time measurement equation is

$$Y_t = T_{i,t} + e_t, \tag{2}$$

where t is the measurement point in time, Y_t the measured interior temperature and e_t is the measurement error [18], assumed to be Gaussian white noise as the fitted model accurately captures the dynamics of the system. With observations represented by

$$\mathcal{Y}_N = [Y_N, Y_{N-1}, \dots, Y_1, Y_0],$$
 (3)

the maximum likelihood estimates of the grey-box model parameters can be identified from the joint probability density [19]

$$L(\theta; \mathcal{Y}_N) = \left(\prod_{k=1}^N p(Y_k | \mathcal{Y}_{k-1}, \theta)\right) p(Y_0, \theta), \tag{4}$$

where $p(Y_k|\mathscr{Y}_{k-1},\theta)$ represents the conditional density designating the probability of observing Y_k given the preceding observations and the parameters θ , and where $p(Y_0, \theta)$ is a parameterization of the starting conditions. This is done by introducing an expected value of the initial states and the associated covariance matrix. Maximum likelihood estimates of the parameters can then be found from

$$\hat{\theta} = \underset{\theta}{\operatorname{argmax}} \left\{ L(\theta; \mathscr{Y}_{N}) \right\}, \tag{5}$$

which can be calculated using an optimization algorithm over a Kalman filter. We refer to the work of Kristensen et al. [19] for a detailed description of the approach.

2.1.1. Applied models

This study considers grey-box models ranging from the simple first order T_i model, explicitly described in Eq. (7), where the inside temperature state-point T_i and its RC parameters R_{ia} and C_i are solely treated, to 5^{th} order ones, where the addition of sensor T_s , medium T_m , heater T_h and building envelope T_e state points along with their respective RC parameters each add a variety of model extensions to choose from. Additionally, the building envelope component proposes additional parameter extensions modeling direct inside to outside heat exchanges and facade solar gains, which are here considered as a block extension $A_{\rho}R_{ia}$.

The full model $T_i T_m T_e T_h T_s A_e R_{ia}$ is visually displayed in Fig. 1 and the set of stochastic differential equations describing its heat flows in continuous time are [14]

Sensor:
$$dT_{s} = \frac{1}{R_{is}C_{s}}(T_{i} - T_{s})dt + \sigma_{s}d\omega_{s},$$
Interior:
$$dT_{i} = \frac{1}{R_{is}C_{i}}(T_{s} - T_{i})dt + \frac{1}{R_{im}C_{i}}(T_{m} - T_{i})dt$$

$$+ \frac{1}{R_{ih}C_{i}}(T_{h} - T_{i})dt + \frac{1}{R_{ie}C_{i}}(T_{e} - T_{i})dt + \underbrace{\frac{1}{R_{ia}C_{i}}(T_{a} - T_{i})dt}_{R_{ia}\text{component}}$$

$$+ \frac{1}{C}A_{w}\Phi_{s}dt + \sigma_{i}d\omega_{i},$$
(6)

Medium :
$$dT_m = \frac{1}{R_{im}C_m}(T_i - T_m)dt + \sigma_m d\omega_m,$$
 (8)

Heater
$$:dT_h = \frac{1}{R_{ih}C_h}(T_i - T_h)dt + \sigma_h d\omega_h,$$
 (9)

$$\begin{aligned} & \text{Medium } : dT_m = \frac{1}{R_{im}C_m}(T_i - T_m)dt + \sigma_m d\omega_m, \end{aligned} \tag{8} \\ & \text{Heater } : dT_h = \frac{1}{R_{ih}C_h}(T_i - T_h)dt + \sigma_h d\omega_h, \end{aligned} \tag{9} \\ & \text{Envelope } : dT_e = \frac{1}{R_{ie}C_e}(T_i - T_e)dt + \frac{1}{R_{ea}C_e}(T_a - T_e)dt + \underbrace{\frac{1}{C_e}A_e\Phi_s dt}_{A_e\text{component}} + \sigma_e d\omega_e, \end{aligned} \tag{10}$$

where the subscripts s, m, and e point to sensor, medium and envelope components respectively. The discrete time measurement equation is

$$Y_t = T_{s,t} + e_t, \tag{11}$$

as observed temperature is encumbered with measurement error. We refer to an applied model as a combination of its corresponding state-point(s) T_x component and block model component extension $A_e R_{ia}$, highlighted in the under-brackets of Eqs. (7) and (10). For example, the model $T_iT_eT_h$ comprises the first order model T_i with envelope T_e and heater T_h component extensions, but without the inclusion of the $A_e R_{ia}$ block extension of the envelope. For a detailed description of the models, the reader is suggested to refer to the work of Bacher and Madsen [14].

It should be noted that while our approach proposes to apply the RC models put forward by Ref. [14], our proposed automated model selection and evaluation procedure, describe in the following subsection, can be applied to any set of increasing complexity of grey-box models.

2.2. Automated model selection and evaluation procedure

The scaling up of grey-box approaches for automated model selection can be challenging. Initial values of parameters are usually tuned to the case study from expert inspection while model extensions are iteratively built and evaluated. Here we present the proposed model selection and evaluation procedure.

2.2.1. Model selection

The model selection procedure employs a likelihood ratio test to statistically determine whether a more complex model performs significantly better, or not, compared to a simpler, sub-model. Likelihood ratio tests are particularly effective at comparing two competing statistical models with no unknown parameters and have been demonstrated by the Neyman-Pearson lemma to have the highest statistical power amongst all other contestants [20]. This implies that the test is able to make the most efficient use of the available data. A forward selection procedure is proposed beginning with the simplest feasible model, T_i , and extending it iteratively with the component presenting the most significant improvement. The procedure terminates when no model extension yields a p-value below the pre-specified limit, commonly fixed at 5%. Possible candidates for model improvement are selected from a set of predefined extensions, resulting from the combination possibilities of the different considered model components, i.e., $T_e, T_h, T_m, T_s, A_e R_{ia}$. Fig. 2 presents the overall model selection scheme. Possible model combinations are mapped and linked, visually exposing the different existing paths of the forward selection procedure. The process has been adapted from [14] to assure more coherent ranges of evaluated parameters within each iteration phase.

2.2.2. Model evaluation

Finally, we extend the existing model evaluation phase of [14] to render the process suitable for automated deployment. This last step leverages the commonly employed qualitative appreciation of model fits from cumulated periodograms of the residuals. A peri-

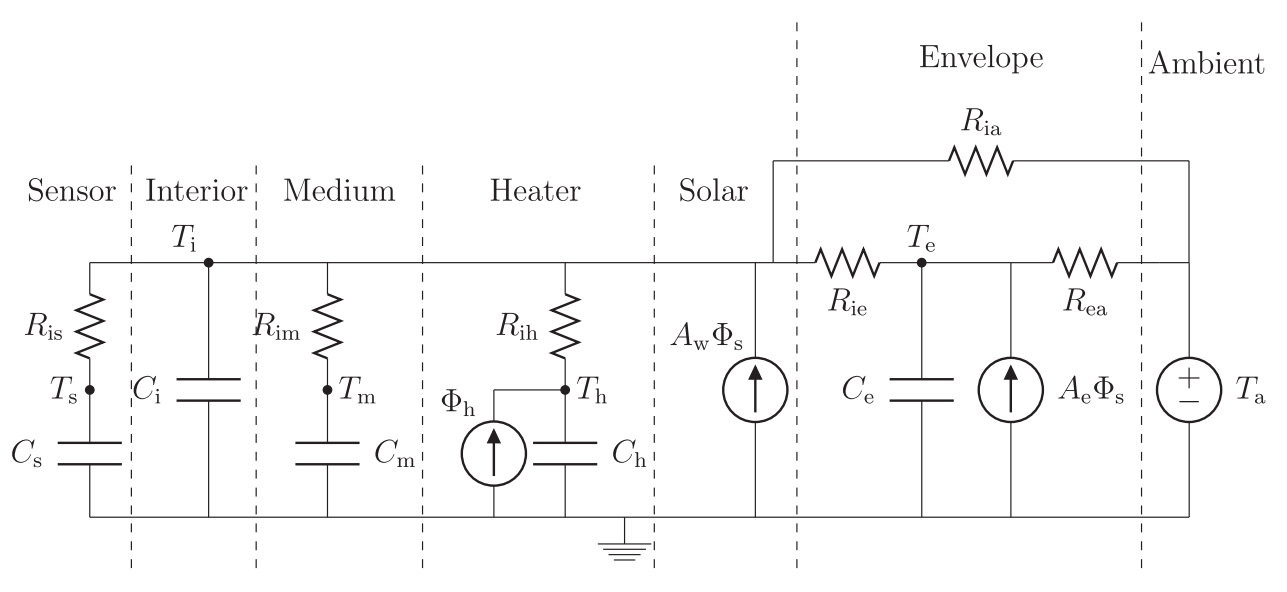


Fig. 1. The full model $T_i T_m T_e T_h T_s A_e R_{ia}$ with all considered model extension parts presented and individually indicated. The model consequently depicts all parts included in any of the other applied models. Reprinted from the work of Bacher and Madsen [14] with the authors approval.

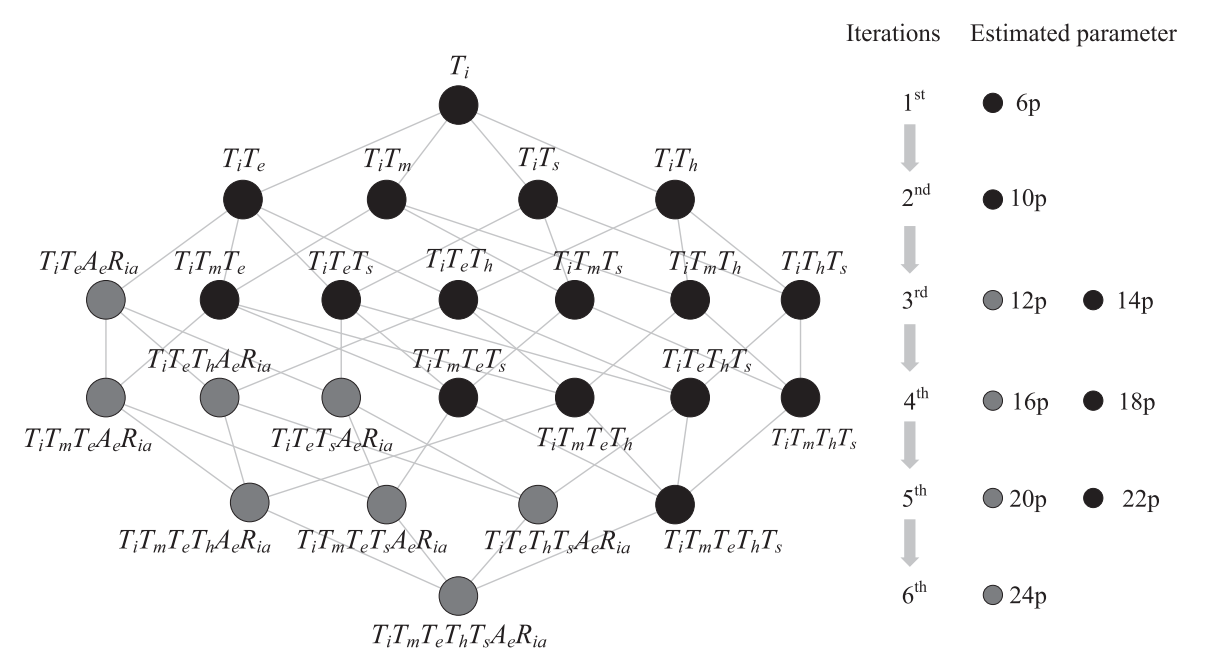


Fig. 2. Forward model selection scheme.

odogram, or sample spectrum, is obtained by Fourier transforming the autocovariance function of a stationary process [21]. Typically, an appropriate model will produce residuals with Gaussian whitenoise properties, which in the frequency domain, denotes a theoretical constant periodogram [21]. Observing whether obtained model residuals are located around this straight line, e.g. within a surrounding confidence interval, consequently serves as an appropriate indicator of a model's quality.

By calculating the frequency differences between a selected model's Cumulated Periodogram (CP) and its confidence interval, we obtain boundary excess values which, in turn, can be summed into a unique numerical indicator, i.e., the Cumulated Periodogram Boundary Excess Sum (CPBES). This indicator characterizes the amount of auto-correlation present in the considered input timeseries, which implies white noise properties when close to zero.

CPBES consequently allows the differentiation of poor, suitable and good models resulting from the previous forward selection procedure. To allow fair comparisons of CPBES between times series of different lengths we normalize it by length and obtain the normalized CPBES (nCPBES).

Quite concretely, the CP is calculated from the normalized sum of the Discrete Fourier Transform (DFT) of the time series

$$CP(k) = \frac{1}{K} \sum_{i=1}^{k} |DFT(x_j)|^2.$$
 (12)

Here *x* denotes the input time series, *k* the considered Fourier frequency of the periodogram, and *K* is the last Fourier frequency of the domain, which corresponds to the times series length, i.e. *N*, minus one. The periodogram confidence interval, or boundaries

(B), are obtained from the Kolmogorov–Smirnov test for distributions at a given probability $(1 - \alpha)$ [21]. The obtained bounds are characterized from the slope and intersection coefficients

$$B_{intersect} = \sqrt{2} \cdot K_{\alpha} \cdot \left(\frac{K-1}{2} - 1\right)^{-1/2}, \tag{13} \label{eq:13}$$

$$B_{slope} = 2T, (14)$$

where K_{α} is equal to 1.358 for confidence intervals of 95%, and T corresponds to the period, or the frequency inverse, of the input time-series [22]. Finally the nCPBES can be determined from:

warm summer regions. Anonymized measurements are collected from the Toon smart-thermostats proposed by the energy distributor Eneco, with whom this work was carried out in collaboration. Measured data include inside temperature and boiler (heater) setpoint temperature, at granularities of 15 min intervals. Few building meta-data are made available by users as self-reported information such as building type, floor surface and family size.

Boiler set-point temperature can here be considered to act as the centralized space heating input signal of buildings. Indeed, centralized heating systems of dwellings are commonly operated by adjusting delivery temperatures, i.e., measured (boiler) set-point temperature, while a pump maintains a constant pressure across

$$CPBE(k) = \underbrace{max(0, CP(k) - B_{slope} \cdot k - B_{intersect})}_{top boundary excess} + \underbrace{max(0, B_{slope} \cdot k - B_{intersect} - CP(k))}_{bottom boundary excess}, \tag{15}$$

$$nCPBES = \frac{1}{K} \underbrace{\sum_{k=1}^{K} CPBE(k)}_{CPBES}.$$
 (16)

Fig. 3, illustrates how nCPBES is obtained from a given cumulated periodogram. It should be noted than while nCPBES is suited for automated model selection as a unique numerical indicator, its cumulated periodogram or derived boundary excess curve still present valuable qualitative information, indicating the frequencies of the dynamics the model is not capturing. These can be employed for in depth model analysis a posteriori to the automated model selection process. For instance, the boundary excess curve of Fig. 3 presents two lumps located around frequencies of 0.2 and 0.4 (2/h) which correspond to periods of 10 and 5 h respectively. This allows the analyst to identify the frequencies of the dynamics still present in the residuals which can later drive the design of model extensions or suggest the need for additional measurements.

3. Implementation

Our study considers a total of 247 homes located in the Netherlands, a European region under the Köppen climate classification index [23] *Cfb* which describes mild temperate, fully humid and

the building's pipelines. This setup implies eventual non homogeneous power outputs throughout radiators, should their combined valve positions be readjusted, even with fixed boiler set-point temperatures. Commonly, though, radiator valves are set to fix positions by building occupants and house temperature is adjusted directly from the thermostat. Such variations can therefore be considered negligible and the boiler set-point a good indicator of space heating input signal.

Hourly weather data are collected from the publicly available Royal Netherlands Meteorological Institute (KNMI) weather stations [24]. Stations are paired to each building thanks to a geolocalisation process using 4 (over the 6) ZIP code digits; an aggregation level that allows no anonymized user to be geographically isolated nor identified. Fig. 4 shows the distribution of distances between the building's province and its nearest KNMI station. Obtained distances are centered principally between 5 and 12 km, while a few larger distances can be found above 20 km. While these measurements cannot encapsulate local weather conditions particular to micro urban surroundings, they provide a sufficient approximation of building outside conditions.

To capture the thermal dynamics of a building, we consider minimum measurement periods of 2 months and limit the maximum times-series horizon to 4 months. We filter available data to obtain the most recent continuous measurement period for each

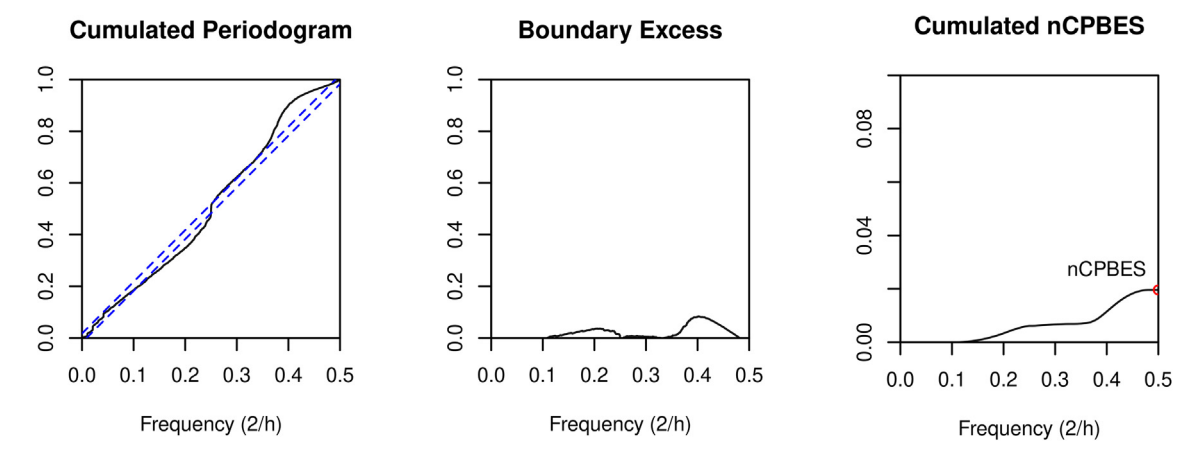


Fig. 3. Model residual cumulated periodogram transformed to normalized Cumulated Periodogram Boundary Excess Sum (nCPBES) for automated model evaluation.

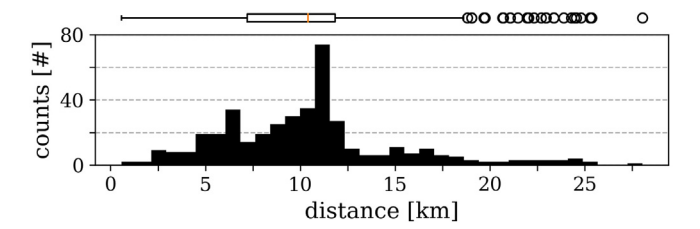


Fig. 4. Distance distribution between building province and its nearest KNMI weather station, showcasing both a boxplot (top) and histogram (bottom) for a more informed distribution appreciation.

building resulting in periods ranging from February 1st to the end of May 2021, which holds a notably cold start of spring season at the beginning of April. Weather data are re-sampled to 15 min resolutions to fit thermostat measurements. While finer granularities, typically 1 or 5 min, are better suited to capture the thermal dynamics of building systems, 15 min resolutions are sufficient to do so. Cumulative missing values larger than 2 h are imputed while smaller gaps are interpolated via a moving average using a window size of 8 h.

Grey-box models are implemented using the computer software CTSM-R [25] developed at the Technical University of Denmark. It produces maximum likelihood estimates of model parameters thanks to an optimization algorithm performed over a Kalman filter. The code developed for this study is made available under an open-access github repository, i.e. https://github.com/JulienLeprince/fiftyshadesofgrey, to encourage dissemination and support its reproducibility.

4. Results and discussion

We describe the outcome of the implementation section here with a first model evaluation subsection. Estimated model parameters and highlighted links to building characteristics are then presented, followed by a final illustrative building performance application, leveraging model parameter estimates for city-scale building envelope insights.

4.1. Model evaluation

The normalized cumulated periodogram boundary excess sum indicators are used to differentiate good from close and poor model fits. Fig. 5 presents the cumulated periodogram, boundary excess and nCPBES of all final models obtained from the forward selection procedure. After an attentive inspection of the CPs and their

respective nCPBES, threshold values of 0.3 and 0.1 nCPBES were fixed to differentiate regions of poor, close and good quality fits as illustrated in Fig. 5. In total, 93 models are determined as good fits, 95 as close fits and 59 are categorized as poor fits. It can also be noted that most close fits present boundary excess lumps located around frequencies of 0.15 and 0.4, which indicates that these models are not capturing dynamics occurring at periods of 13 and 5 h respectively. Both these dynamics might be caused by occupant usage of appliances generating heat inputs not covered in the measurements, e.g., kitchen appliances. A 13 h period for instance typically represents daily unoccupied residential kitchen-usage schedules with morning to late evening activities, i.e., 7:00-20:00, while a 5 h period corresponds better to an occupied daily Dutch kitchen-usage schedule, where dinner is prepared rather early, i.e., 7:00-12:00-17:00. In fact, findings from related work, leveraging symbolic regression knowledge discovery on a similar data set, revealed the preferred use of gas-meter measurements over heat input signal for the heat dynamics identification of 24 of these buildings [26]. Indeed, Dutch homes typically employ gas to supply both space heating and kitchen appliance needs. This underlines the impact and importance of these appliances on building heat inputs.

The forward selection paths adopted in the model selection phase are illustrated in Fig. 6. These display an overall even distribution of models amongst the $2^{\rm nd}$ iteration phase, with a slight preference for T_iT_h models, while in the $3^{\rm rd}$ iteration phase, $T_iT_mT_s$ comes out as the most likely choice. This seems to indicate favored additional degrees of freedom around the inside temperature in the forward selection procedure. It can be noted that only one $A_eR_{i\alpha}$ envelope extension is selected out of the $2^{\rm nd}$ iteration phase, yet more envelope model extensions are preferred in the later phases of the selection. The $4^{\rm th}$ iteration distinctly denotes $T_iT_mT_eT_s$ as the most preferable choice, yielding a consequent share of final models. Finally, the $5^{\rm th}$ and $6^{\rm th}$ iterations largely compose final selected models with little to be noted from their selection paths.

Identified models are presented in Fig. 7 along with their residual standard deviation, parameter significance, proportions of fit quality as well as available building meta-information, i.e. home size, home type and family size, which will be discussed in the following sub-section. Firstly, the standard deviations of obtained model residuals serve to illustrate the amplitude of forecasting errors produced. These range between values of 0.05 and 2°C for the most extreme cases, and possess central tendencies grouped between values of 0.1 and 0.2°C. The grouping of residual standard deviations per model fit quality (top Fig. 7) clearly demonstrates a decrease in residual amplitude as the fit increases in quality,

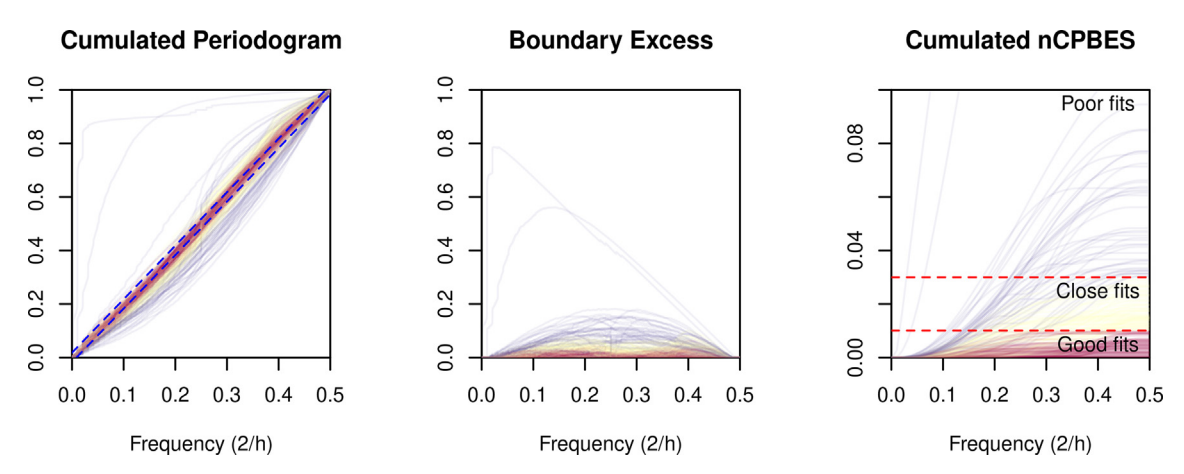


Fig. 5. Models residual cumulated periodograms, boundary excess curves and cumulated nCPBES.

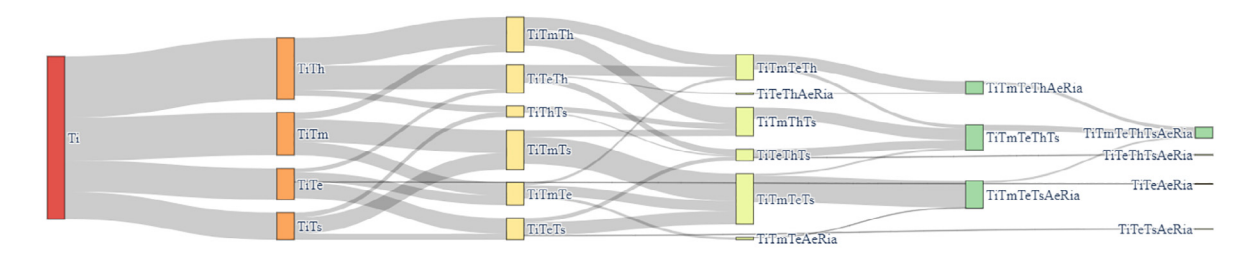


Fig. 6. Flow diagram of forward model selection paths. The figure presents flows and nodes to illustrate the selection path of models, with their width being proportional to the number of final models using this selection path. A final selected model $T_i T_e T_h$ for instance, could be obtained by a selection path either following $T_i > T_i T_h > T_i T_e T_h$ or $T_i > T_i T_e > T_i T_e T_h$. The width of the flows entering the designated $T_i T_e T_h$ node is therefore proportional to the number of final models considering the $T_i T_e T_h$ model in their forward selection path. Nodes may possess fewer number of flows exiting it (right-hand side) than entering it (left-hand side). Taking the same example of the $T_i T_e T_h$ node, this means the model $T_i T_e T_h$ was considered final for a number of cases proportional to the missing existing flow of the node. As the selection procedure moves forward (from left to right), fewer flows are represented as more and more models are identified as final in earlier stages, consequently making the presented selection path-flows non-conservative over the flow diagram.

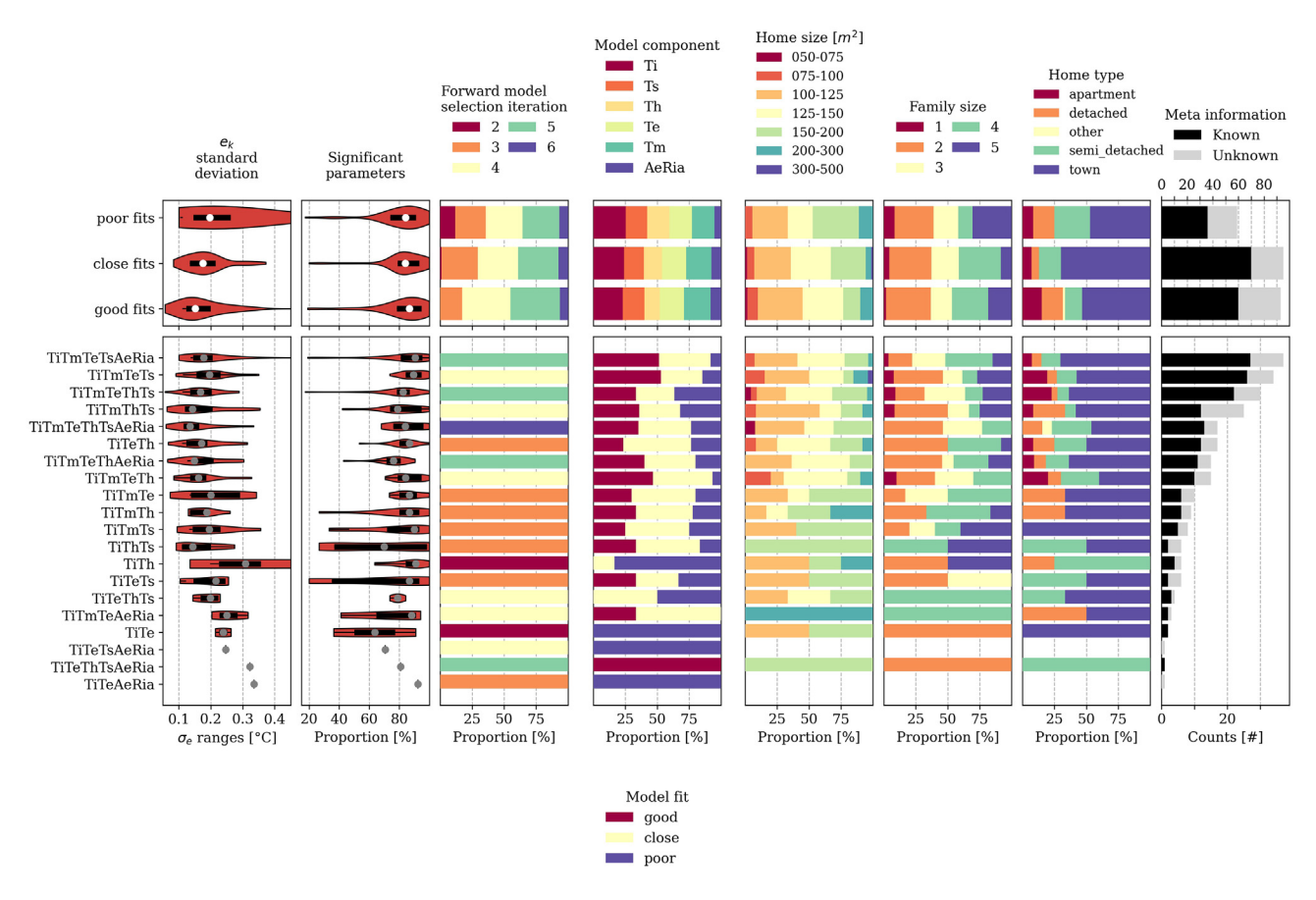


Fig. 7. Identified models grouped per fit quality (top) and thermal model (bottom) with their respective residual standard deviation distribution, parameter significance, iteration phase, modeling components (top) or model fit quality (bottom), meta-data proportions and counts. Residuals' standard deviation values are displayed from violin plots in panel one, while panel two depicts in a similar manner the distribution of parameter significance proportions per group. Panel three shows the iteration phase in which the forward model selection procedure stopped, which are logically homogeneous for any given individual model (bottom panel). Panel four presents either the proportion of model components across the groups (top) or model fit quality (bottom), as these are insights specific to their opposing panel. Panels five to seven offer the proportions of available meta-data information as self-reported by occupants, namely home-size, family-size and home-type. Lastly, panel eight displays each groups' respective number of members while highlighting the portion of meta information self-reported, or not, within them.

although a larger tail persists amongst good model fits, compared to close ones. It should be noted, however, that residual amplitudes are an indication of the degree of noise variations present in the measurements, and are independent from residual covariance, i.e., model fit quality. A residential home with 4 occupants might result in a larger amount of noise, i.e., higher standard deviations, while possessing a thermal model accurately capturing all of its

dynamics, with residuals demonstrating white noise properties, i.e., nCPBES close to zero. The aforementioned observation consequently comes rather as a fortuity than the result of a correlation between these two features. Secondly, parameter significance reveals whether estimated model parameters exhibit substantially likely probabilities and support the evaluation of model robustness. The comparison of parameter significance grouped by model

fit quality shows that good fits present slightly larger central tendencies of significant parameter proportions compared to poor and close fits, although all three groups present similar distribution tails reaching down to 20%. Thirdly, the forward model selection iteration phase proportions show no 1st order model selected as best fit in either of the categories, and no 2nd order models are either present in close and good model fits. This finding confirms our initial assumptions that first- and second-order models would not be sufficient to capture thermal dynamics of buildings. The iteration proportions clearly display larger iteration phases becoming more important from poor to good model fits, suggesting that to obtain a good fit it is likely the model will be more complex. Lastly, it is found that the four most considered models are $T_i T_m T_e T_s A_e R_{ia}$, $T_i T_m T_e T_s$, $T_i T_m T_e T_h T_s$ and $T_i T_m T_h T_s$, which all employ the sensor, T_s , and medium, T_m , model components. The two largest of them notably possess the greatest proportion of good fits, reaching 50%, while being sensibly similar models with common components T_i, T_m, T_e and T_s .

4.2. Parameters and building characteristics

Identified parameters and models coupled with available building characteristics constitute a valuable examination analysis that has the potential to unveil meta-data links to exposed building thermal dynamics. Estimated RC parameters are presented per model component under Fig. 8 with highlighted model quality fit and parameter significance. It displays thermal capacities of sensor and heater components as relatively aggregated around 0 kWh/K, while medium and envelope capacities are relatively split between their lower upper bound values, 0 and 20 kWh/K respectively. On the other hand, resistance estimates are mostly comprised between values of 0 to 5 K/kW at the exception of $R_{i\alpha}$ which spreads quite evenly from 0 to 50 K/kW. The scatters show no apparent correlation between estimated parameter values and their relationship to fit quality or significance.

The building meta-data distributions of Fig. 7 reveal that poor to good model fits possess increasing proportions of smaller home sizes along with larger shares of family sizes of 2. This supports the intuitive thought that smaller, thus simpler, residential homes are more likely to result in good model fit.

4.3. Building envelope performance

Identified building heat dynamics can be leveraged to calculate building envelope insulation properties such as the Heat Transfer Coefficient (HTC). HTC is defined in ISO 13789:2017 [27] as the heat flow rate from the internal air mass to the surrounding exter-

nal environment divided by the indoor-outdoor air temperature difference [28]. Its estimation is obtained from the sum of heat flow rates due to ventilation UA_V , and transmission UA_T , which includes plane building envelope elements as well as thermal bridges. Linking these elements to the identified thermal resistances R of the model, the HTC can be derived from [10]

$$HTC = \underbrace{\frac{UA_T}{1}}_{\frac{1}{UA_L} + \frac{1}{UA}} + \underbrace{UA_{ia}}_{UA_{ia}} \left(WK^{-1}\right), \tag{17}$$

$$HTC = \frac{1}{R_{ie} + R_{ea}} + \underbrace{\frac{1}{R_{ia}}}_{\forall T_e \in \mathbb{M}} + \underbrace{\frac{1}{R_{ia}}}_{\text{or}} \underbrace{\left(WK^{-1}\right)}, \tag{18}$$

where \mathbb{M} stands for the model component ensemble of the final selected model. HTC can be expressed in absolute units, i.e., \mathbb{W}/\mathbb{K} as defined above, or in useful floor area relative units, i.e., $\mathbb{W}/(\mathbb{K}\cdot\mathbb{m}^2)$ as recalled in ISO 52016:2017 [29] with

$$HTC_{norm} = \frac{HTC}{A_{use}} \left(WK^{-1}m^{-2} \right), \tag{19}$$

where HTC_{norm} refers to the area normalized HTC and A_{use} to the total useful floor area of the considered building. The latter naturally being better suited to benchmark insulation performances thanks to building floor surface independence.

With useful floor area unavailable across this study's building stock however, we proceed to identify absolute building HTCs and total thermal capacities jointly. This allows a relatively fair comparison of building thermal properties together. Indeed, investigating these parameters by pair presents the advantage of providing a complete overview of a building stocks' thermal properties. The inclusion of total thermal masses in this frame puts the absolute HTC into perspective while providing an efficient way to identify groups of similar buildings, as well as singling-out poorly insulated home envelopes for instance. Fig. 9 presents these identified characteristics along with highlighted building type and poor quality fits. Results show a strong concentration of total thermal capacities between values of 20 and 24 kWh/K with few values reaching above 40 kWh/K and below 10 kWh/K. HTCs present a strong positively skewed distribution, mostly concentrated between 0.02 to 0.05 kW/K, with a smaller peak centered around 0.1 kW/K. The scatter reveals a main cluster of points originating from the strong concentrations of both thermal parameters around their central distributions. Building types do not appear correlated to the presented thermal properties. A larger share of isolated dwellings (town building type) are present at the center of the cluster, yet their vast larger proportion within the data set biases this

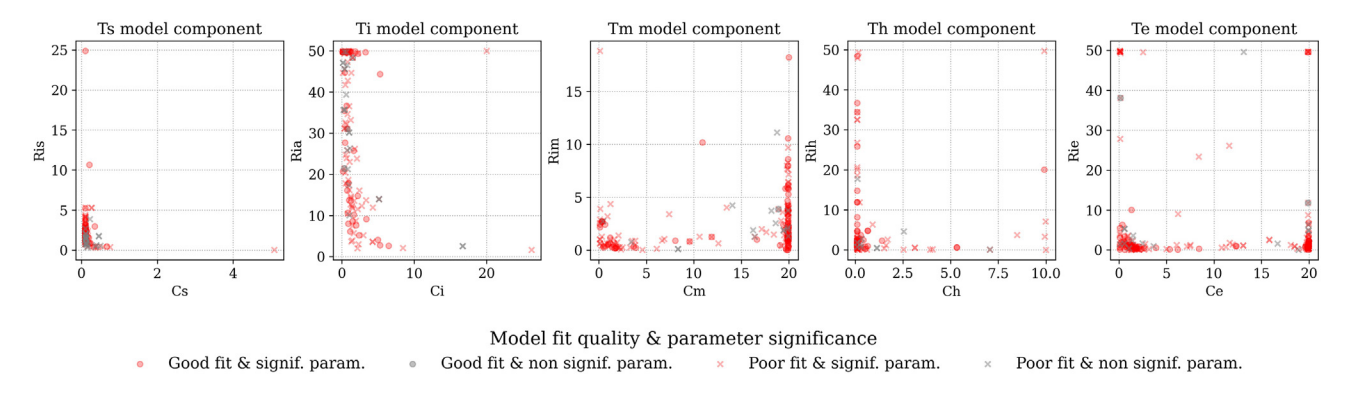


Fig. 8. Scatter plots of RC parameter estimated per model component, with model fit quality and parameter significance. Good from poor model fits are differentiated, where close fits are here grouped together with poor fits, while the scatter point crossover between two parameters will be considered significant only if both represented parameters are so.



poor model fit

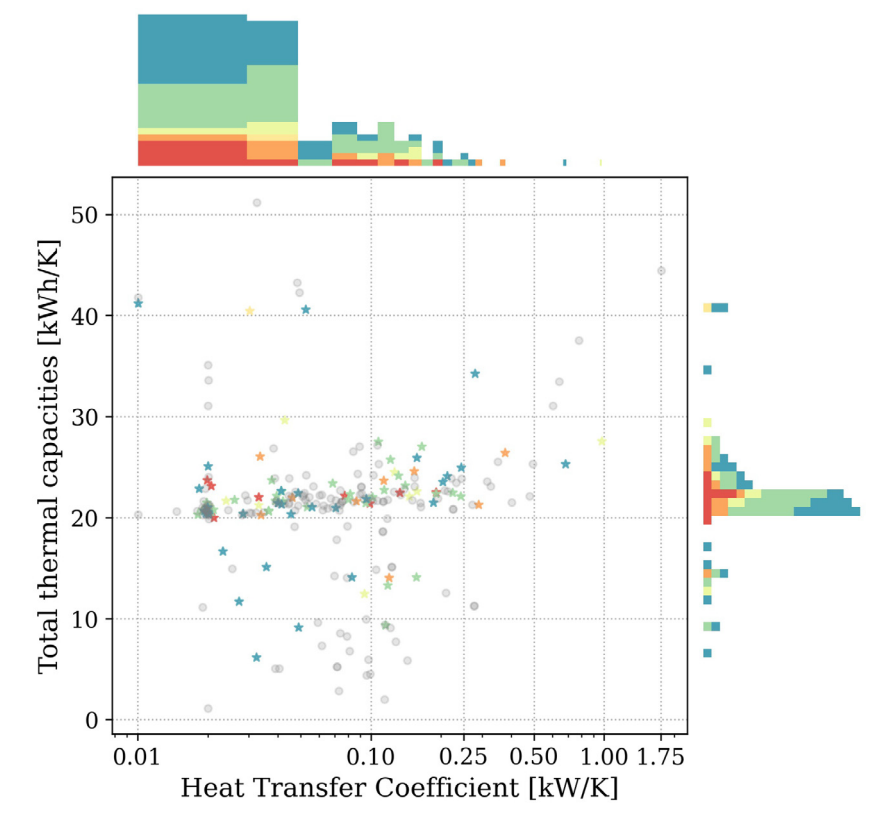


Fig. 9. Scatter plot of building envelope Heat Transfer Coefficient (HTC) versus sum of total heat capacities, with highlighted building types. Poor model fits here englobe both close and poor fits.

observation. Identified good model fits presenting HTC values above 0.20 kW/K can thus be considered of poor thermal insulation. This constitutes a non-intrusive, scalable and quite simple building envelope characterization which can support city-scale building stock analytics. Retrofit potentials could consequently be evaluated from the granted insights and provide users with impactful energy saving opportunities from recommended insulation upgrades.

5. Applications and outlooks

The development of methods that focus on the scalability of analysis across the building stock unlocks the potential of several important applications. The results of this method illustrate its effectiveness on a set of buildings that could be replicated in other contexts. This section outlines a review of those results related to several applications.

5.1. Building performance benchmarking

Benchmarking the building stock enables the owners and occupants to understand how their building compares to its *peers*. Defining just what a peer is for a certain building is a challenge in itself. A certain amount of metadata, or characteristic attributes are necessary to undertake fair benchmarks between buildings. Notable building geometry-related characteristics proportionally influencing heating and cooling demands encompass area to volume ratios such as shape factor, i.e., an envelope surface to heated volume [30] or surface [31] ratio. Yet the collection of these information at scale is tedious [32]. The automated creation of dynamic models could enhance this process by enriching existing metadata with identified building thermal properties [33], ranging from

model structures to parameter estimates which could be employed within the benchmarking process.

For instance, building performances are typically evaluated from key performance indicators (KPI) such as CO₂ emissions reductions, energy costs savings, energy balance, thermal/light comfort, system efficiency or peak demand reduction [34]. A common approach employed to compare the energy performance of a heterogeneous building set consists in area-normalizing their respective energy consumption [35]. However, floor surface does not provide a complete characterization of a building's thermal mass. Knowledge of buildings thermal capacities can provide a much richer description of their heating and cooling inertiae for fairer thermal load comparisons. Building thermal capacities C can either encapsulate their internal environment with units in J/ K, or air and furniture areal capacity considering units of $J/(K \cdot m^2)$ [29]. The latter, similarly to HTC_{norm} , includes useful floor area information and can serve in benchmarks for the consideration of not only building thermo-physical properties, but also geometry. When undertaking such energy performance benchmarks, heating and cooling demands Φ_d could consequently be normalized as follows.

$$\Phi_{d,norm} = \frac{\Phi_d}{\sum_{i} C_j} \tag{20}$$

where $\Phi_{d,norm}$ here either stands for the internal environment capacity normalized heat load of a building, with C in J/K and $\Phi_{d,norm}$ in K/s, or the air and furniture areal capacity normalized heat load, with C in J/(K·m²) and $\Phi_{d,norm}$ in km²/s. The subscript j refers to the components of the fitted grey-box model.

This scaling approach makes it possible to compare design assumption, i.e., useful floor area, with field performance, i.e.,

heating/cooling demands, at scale. Indeed, through the inclusion of building geometry information in the scaling process of identified thermal characteristics, it becomes possible to compare actual building thermo-physical properties to design parameters from technical standards on a building stock level.

5.2. Building stock scenario modeling

One of the key benefits of white box modeling is the ability to test possible future scenarios of performance enhancement [36]. Undertaking this effort on a large building stock is a significant challenge [37]. The automated creation of physics-informed models enables this in a scalable and effective way, allowing renovation influences or policy decisions impact assessments up-to a city or district-scale. This type of effort has been explored on non-residential buildings in the direction of inference of higher granularity data from annual and district-level public data [38]. Quite concretely, one could imagine varying identified HTC distributions within the building stock to predict insulation renovations impact on thermal loads.

5.3. Decomposition of energy meter into end-use loads at a city-level

The integration of more dynamic influences on energy grids from renewable sources such as wind and solar have a significant impact on their operation. The ability to characterize, at scale, energy consuming dynamics of large numbers of buildings can improve optimal grid operations. Policies aiming at enhancing grid stability using technologies like storage unavoidably profit from more accurate energy demand characterizations [39]. Additionally, the decomposition of energy-meter information into load influencing factors sets the foundations to factor-dependent energy predictions, which support scenario-specific predictions at city-level. For example, with identified climate's influence on overall building stock load one could predict how a city's energy demand might change under varying weather scenarios, or account for perfactor uncertainties in forecasted values for a resilient and optimal operation of the energy system. Further innovations in this direction can support efforts from the literature focusing on model development using large, open data sets from energy disclosure programs [40,41] or from geospatial sources [42] for instance.

5.4. Demand side management

Identified thermal dynamics may also be leveraged to evaluate the energy flexibility potential of buildings. Indeed, the derivation of a system's time constants, which characterize the dynamic response of the considered system, can be determined based on estimated parameters [18]. These time constants can notably provide information about the building's reaction to affecting variable changes, namely weather conditions and heat inputs. The work of [33] exemplifies this process on a data set of 39 Danish residential buildings. From identified thermal dynamics it formally links estimated time constants to each building's energy flexibility potential. Proposing scalable methods to evaluate the dynamic response of the building stock is a crucial step that our work opens the door to for developing more effective demand-side management strategies.

6. Conclusion

This work puts forward an automated stochastic model identification approach for building heat dynamics, suited for scalable deployment. It proposes a forward model selection procedure adapted from [14] and extended with a novel residual auto-

correlation indicator, i.e. the normalized Cumulated Periodogram Boundary Excess Sum (nCPBES). This indicator allows automated classification of identified models into groups of fit-quality. Out of the 247 buildings the approach was tested on, 93 model fits were identified as good, 95 were classified as close while 59 were designed as poor. Good model fits presented overall larger shares of model complexities and parameter significance along with smaller reported building surfaces and family sizes compared to poor and close model fits. Estimated RC parameters presented no notable tendencies when compared to model fit qualities or their significance. We examined thermal properties of the building stock by visualizing their total thermal capacities and respective HTC. A main cluster of buildings with similar properties is clearly observed suggesting a large share of buildings possessing similar thermal characteristics. Finally, we discussed how the proposed approach is valuable to the building sector. In particular, how automation and scalable solutions for building stock model identification can support in an unprecedented way applications such as building performance benchmarks, city-scale scenario modeling, energy dissagregation to building end-loads and large scale demand-side management.

CRediT authorship contribution statement

Julien Leprince: Conceptualization, Methodology, Data curation, Formal analysis, Visualization, Writing - original draft, review & editing. **Henrik Madsen:** Methodology, Supervision, Validation, Writing - review & editing. **Clayton Miller:** Supervision, Writing - review & editing. **Jaume Palmer Real:** Writing - review & editing. **Rik der Vlist:** Data curation. **Kaustav Basu:** Data curation. **Wim Zeiler:** Supervision, Funding acquisition.

Declaration of Competing Interest

The authors declare that they have no known competing financial interests or personal relationships that could have appeared to influence the work reported in this paper.

Acknowledgments

This work is funded by the Dutch Research Council (NWO), in the context of the call for Energy System Integration & Big Data (ESI-bida). Support by Flexible Energy Denmark (IFD, No. 8090-00069B), Research Centre on Zero Emission Neighbourhoods in Smart Cities - FME-ZEN (Research Council of Norway, No. 2576609), and FlexBuild (Research Council of Norway, No. 294920) are also gratefully acknowledged. Finally, we wish to express our appreciation of the support and contribution of Eneco as well as Eneco customers to this research.

References

- I.E.A., the United Nations Environment Programme (2019), 2019 global status report for buildings and construction: Towards a zero-emission, efficient and resilient buildings and construction sector (Dec 2019). URL:https:// www.worldgbc.org/sites/default/files/2019 Global Status Report for Buildings and Construction.pdf..
- [2] M. Rabani, H.B. Madessa, N. Nord, A state-of-art review of retrofit interventions in buildings towards nearly zero energy level, Energy Procedia 134 (2017) 317–326, sustainability in Energy and Buildings 2017: Proceedings of the Ninth KES International Conference, Chania, Greece, 5–7 July 2017. doi: 10.1016/j.egypro.2017.09.534. URL:https://www.sciencedirect.com/science/ article/pii/S1876610217346635..
- [3] E. Guelpa, V. Verda, Demand response and other demand side management techniques for district heating: A review, Energy 219 (2021), https://doi.org/ 10.1016/j.energy.2020.119440, URL:https://www.sciencedirect.com/science/ article/pii/S0360544220325470 119440.
- [4] Y. Wang, Q. Chen, T. Hong, C. Kang, Review of smart meter data analytics: Applications, methodologies, and challenges, IEEE Trans. Smart Grid 10 (2019) 3125–3148.

- [5] J. Drgona, J. Arroyo, I. Cupeiro Figueroa, D. Blum, K. Arendt, D. Kim, E.P. Ollé, J. Oravec, M. Wetter, D.L. Vrabie, L. Helsen, All you need to know about model predictive control for buildings, Annual Reviews in Control 50 (2020) 190–232, https://doi.org/10.1016/j.arcontrol.2020.09.001, URL:https://www.sciencedirect.com/science/article/pii/S1367578820300584.
- [6] Z. Wang, T. Hong, Reinforcement learning for building controls: The opportunities and challenges, Appl. Energy 269 (2020) 115036.
- [7] M. Bourdeau, X. qiang Zhai, E. Nefzaoui, X. Guo, P. Chatellier, Modeling and forecasting building energy consumption: A review of data-driven techniques, Sustainable Cities and Society 48 (2019) 101533. doi: 10.1016/j. scs.2019.101533. URL:https://www.sciencedirect.com/science/article/pii/ S2210670718323862.
- [8] D.B. Crawley, L.K. Lawrie, C.O. Pedersen, F.C. Winkelmann, Energy plus: energy simulation program, ASHRAE journal 42 (4) (2000) 49–56.
- [9] S.E. Mattsson, H. Elmqvist, M. Otter, Physical system modeling with modelica, Control Engineering Practice 6 (4) (1998) 501–510.
- [10] X. Yu, L. Georges, L. Imsland, Data Pre-Processing and Optimization Techniques for Stochastic and Deterministic Low-Order Grey-box Models of Residential Buildings, Energy Build. 236 (2021), https://doi.org/10.1016/j. enbuild.2021.110775 110775.
- [11] L. Berti-Equille, Measuring and modelling data quality for quality-awareness in data mining, in: Quality measures in data mining, Springer, 2007, pp. 101– 126..
- [12] J.A. Crabb, N. Murdoch, J.M. Penman, A simplified thermal response model, Building Services Engineering Research and Technology 8 (1) (1987) 13–19. arXiv: 10.1177/014362448700800104, doi:10.1177/014362448700800104. URL: 10.1177/014362448700800104.
- [13] A. Afram, F. Janabi-Sharifi, Review of modeling methods for HVAC systems, Appl. Therm. Eng. 67 (1–2) (2014) 507–519, https://doi.org/10.1016/j. applthermaleng.2014.03.055.
- [14] P. Bacher, H. Madsen, Identifying suitable models for the heat dynamics of buildings, Energy Build. 43 (7) (2011) 1511–1522, https://doi.org/10.1016/j. enbuild.2011.02.005.
- [15] M.M. Hossain, T. Zhang, O. Ardakanian, Identifying grey-box thermal models with Bayesian neural networks, Energy Build. 238 (2021), arXiv:2009.05889, doi:10.1016/j.enbuild.2021.110836. URL: 10.1016/j.enbuild.2021.110836
- [16] A.-H. Deconinck, S. Roels, Is stochastic grey-box modelling suited for physical properties estimation of building components from on-site measurements?, Journal of Building Physics 40(5) (2017) 444–471, https://doiorg/10.1177/ 1744259116688384, arXiv: 10.1177/1744259116688384.
- [17] C. Rasmussen, P. Bacher, D. Cali, H.A. Nielsen, H. Madsen, Method for scalable and automatised thermal building performance documentation and screening, Energies 13 (15). doi:10.3390/en13153866. URL:https://www.mdpi.com/ 1996-1073/13/15/3866.
- [18] H. Madsen, J. Holst, Estimation of continuous-time models for the heat dynamics of a building, Energy Build. 22 (1995) 67–79.
- [19] N.R. Kristensen, H. Madsen, S.B. Jørgensen, Parameter estimation in stochastic grey-box models, Automatica 40 (2) (2004) 225–237, https://doi.org/10.1016/ j.automatica.2003.10.001, URL:https://www.sciencedirect.com/science/ article/pii/S000510980300298X.
- [20] J. Neyman, E.S. Pearson, Ix. on the problem of the most efficient tests of statistical hypotheses, Philosophical Transactions of the Royal Society of London. Series A, Containing Papers of a Mathematical or Physical Character 231 (694-706) (1933) 289–337..
- [21] H. Madsen, Time series analysis, Chapman and Hall/CRC, 2007.
- [22] P.J. Brockwell, R.A. Davis, Time series: theory and methods, Springer Series, Statistics (1991).
- [23] D. Chen, H.W. Chen, Using the köppen classification to quantify climate variation and change: An example for 1901–2010, Environmental Development 6 (2013) 69–79, https://doi.org/10.1016/j.envdev.2013.03.007, URL:https://www.sciencedirect.com/science/article/pii/S2211464513000328.

- [24] KNMI, Hourly values of weather stations (Aug 2021). URL:https://www.daggegevens.knmi.nl/klimatologie/uurgegevens..
- [25] R. Juhl, J.K. Moller, H. Madsen, ctsmr continuous time stochastic modeling in r (2016). arXiv:1606.00242...
- [26] J. Leprince, C. Miller, M. Frei, H. Madsen, W. Zeiler, Fifty shades of black: uncovering physical models from symbolic regressions for scalable building heat dynamics identification, in: Proceedings of the 8th ACM International Conference on Systems for Energy-Efficient Buildings, Cities, and Transportation, BuildSys '21, Association for Computing Machinery, New York, NY, USA, 2021, pp. 345–348..
- [27] Thermal performance of buildings Transmission and ventilation heat transfer coefficients – Calculation method, Standard, International Organization for Standardization, Geneva, CH (Jun. 2017)...
- [28] M. Li, D. Allinson, K. Lomas, Estimation of building heat transfer coefficients from in-use data: impacts of unmonitored energy flows, International Journal of Building Pathology and Adaptation..
- [29] Energy performance of buildings Energy needs for heating and cooling, internal temperatures and sensible and latent heat loads, Standard, International Organization for Standardization, Geneva, CH (Jun. 2017).
- [30] G. Feng, S. Sha, X. Xu, Analysis of the building envelope influence to building energy consumption in the cold regions, Procedia Engineering 146 (2016) 244–250.
- [31] K. Lylykangas, Shape factor as an indicator of heating energy demand, in, in: Proceedings of the 15th International Wood Construction Conference (IHF), 2009
- [32] Y.-Y. Zhang, Z.-Z. Hu, J.-R. Lin, J.-P. Zhang, Linking data model and formula to automate kpi calculation for building performance benchmarking, Energy Reports 7 (2021) 1326–1337, https://doi.org/10.1016/j.egyr.2021.02.044, URL: https://www.sciencedirect.com/science/article/pii/S2352484721001426.
- [33] J. Palmer Real, C. Rasmussen, R. Li, K. Leerbeck, O.M. Jensen, K.B. Wittchen, H. Madsen, Characterisation of thermal energy dynamics of residential buildings with scarce data, Energy Build. 230 (2021) 110530, https://doi.org/10.1016/j.enbuild.2020.110530, URL:https://www.sciencedirect.com/science/article/pii/S0378778820317503.
- [34] Y. Li, J. O'Donnell, R. García-Castro, S. Vega-Sánchez, Identifying stakeholders and key performance indicators for district and building energy performance analysis, Energy Build. 155 (2017) 1–15, https://doi.org/10.1016/j. enbuild.2017.09.003.
- [35] C. Miller, F. Meggers, Mining electrical meter data to predict principal building use, performance class, and operations strategy for hundreds of nonresidential buildings, Energy Build. 156 (2017) 360–373.
- [36] C.F. Reinhart, C. Cerezo Davila, Urban building energy modeling a review of a nascent field, Build. Environ. 97 (2016) 196–202.
- [37] J. Sokol, C. Cerezo Davila, C.F. Reinhart, Validation of a bayesian-based method for defining residential archetypes in urban building energy models, Energy Build. 134 (2017) 11–24.
- [38] J. Roth, A. Martin, C. Miller, R.K. Jain, SynCity: Using open data to create a synthetic city of hourly building energy estimates by integrating data-driven and physics-based methods, Appl. Energy 280 (2020) 115981.
- [39] T. Kerdphol, K. Fuji, Y. Mitani, M. Watanabe, Y. Qudaih, Optimization of a battery energy storage system using particle swarm optimization for standalone microgrids, Int. J. Electr. Power Energy Syst. 81 (2016) 32–39.
- [40] B. Howard, L. Parshall, J. Thompson, S. Hammer, J. Dickinson, V. Modi, Spatial distribution of urban building energy consumption by end use, Energy Build. 45 (2012) 141–151.
- [41] R.K. Jain, K.M. Smith, P.J. Culligan, J.E. Taylor, Forecasting energy consumption of multi-family residential buildings using support vector regression: Investigating the impact of temporal and spatial monitoring granularity on performance accuracy, Appl. Energy 123 (2014) 168–178.
- [42] M.C. Silva, I.M. Horta, V. Leal, V. Oliveira, A spatially-explicit methodological framework based on neural networks to assess the effect of urban form on energy demand, Appl. Energy 202 (2017) 386–398.